Electrical resistivity of silver foils under uniaxial shock-wave compression

J. J. Dick and D. L. Styris*

Shock Dynamics Laboratory, Physics Department, Washington State University, Pullman, Washington 99163
(Received 28 August 1974; in final form 6 December 1974)

The electrical resistivity of silver foils 15–25 μm thick was measured during shock-wave compression between sapphire anvils in the pressure range 25–120 kbar. Comparison of isothermal resistivity vs compression from shock measurement to a simple semiempirical calculation of resistivity under hydrostatic compression shows shock data to be consistently higher than hydrostatic results. Shock results depend on purity and thermal history of the silver foils. Deviation between shock and hydrostatic results is attributed to resistivity of vacant lattice sites generated by high-strain-rate plastic deformation in uniaxial shock compression. Estimated vacancy concentrations at 100 kbar are $(1–2)\times10^{-3}$ per lattice site and concentrations vary approximately as the three-halves power of total strain. The high vacancy concentrations may be evidence for dislocation speeds near shear-wave speed. Annealing and microscopy studies of foils recovered after shocking give additional support to the above conclusions.

PACS numbers: 62.50., 72.10.E, 61.70.

I. INTRODUCTION

Measurements of electrical resistance of crystalline materials as a function of pressure can tell us something about properties of ideal lattices and lattice imperfections. This is possible because changes in the ideal lattice can affect resistivity by changing the electron band structure and electron coupling with the lattice vibration spectrum; rudimentary theory exists for comparison with experimental results.[1,2] In addition, changes in number and types of imperfections will affect electron scattering and, hence, resistivity.

Resistance changes in metals due to transient high pressure generated by shock waves have been measured,[3] but there has been no systematic attempt to compare these results with static high-pressure results or theory so that properties of lattice defects under dynamic pressure might be studied. Evidence for shock-induced defect generation is found in a number of metallurgical and annealing studies on metals which were shocked for a short duration and relieved to atmospheric pressure.[4–6] While many defects generated by the shock wave will have annihilated or migrated to sinks before examination, these studies indicate some of the effects which different shock strengths and initial conditions have on the point and line imperfection densities and configurations generated.

Shock-induced resistance changes have been measured for copper, iron, nickel, and ytterbium, as well as manganin alloy.[3,7] Fractional resistance change for a given pressure level is generally greater for shock compression than for hydrostatic compression, though agreement among different shock experimenters has not been good. Material history might be responsible for these discrepancies; unfortunately, few attempts have been made to do experiments on well-characterized material. Good experiments require a well-characterized initial condition of the metal as well as good shock-impedance match between metal and anvil, geometry that assures uniaxial compression, and elimination of perturbations by electrical leads. In addition, careful analysis is necessary to account for thermal effects occurring in shock compression so that comparison can be made with hydrostatic experiments and theories.

In the experiments described in this paper, electrical resistance changes in silver foils were monitored during uniaxial compression by shock waves; foils were 15—25 μm thick. Electrical resistance of silver under hydrostatic compression was previously measured by Bridgman,[2] but no previous studies on silver resistance under shock compression have been published. Dynamic stress levels ranged from 25 to 120 kbar and were generated by high-velocity impact; shock duration was 0.5 μsec. The voltage drop across the foil due to 150 A of current was monitored during this time. In several cases, foil fragments were recovered after the experiment and examined by microscopy and isothermal annealing.

The present work also involved several types of analysis. Using a Debye model of a solid, a method was developed for computing isothermal resistivity as a function of volume. When a single parameter is adjusted to experimental results, the computation agrees closely with the experiments of Bridgman to 30 kbar. This method was also used to correct shock resistivity data to isothermal conditions. Deviations between isothermal data from uniaxial shock compression and calculated hydrostatic results are attributed to resistivity of lattice imperfections generated by plastic deformation in the shock wave.

The purpose of this paper is to present experimental results on shock resistivity of silver foils, to put the isothermal analysis on a firm footing, to consider all possible effects on the resistivity, and to establish credibility of shock-generated defect concentrations deduced.

Presentation will begin with a description of experimental design and procedure followed by analyses needed to reduce acquired data to meaningful forms, results of the experiments and data reduction, and finally a statement of conclusions.

In summary, by careful experimental design and sample preparation, accurate reproducible resistance measurements during shock compression were accomplished. Shock resistivity depends significantly on specimen purity; some dependence on thermal history may also be indicated. An approximate semiempirical

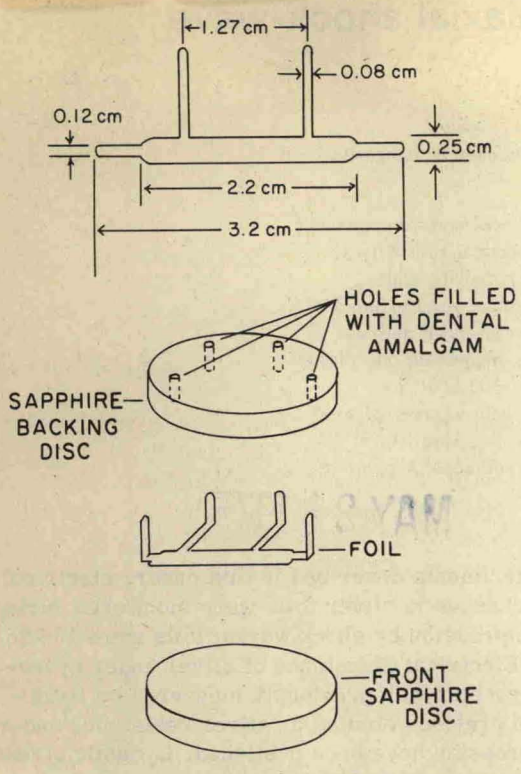

FIG. 1. Details of foil-anvil sandwich. (a) Foil dimensions. (b) Sandwich, exploded view.

resistivity computation allows comparison of hydrostatic and shock isothermal resistivities for silver. Shock results are significantly higher and the deviation is attributed to resistivity of vacant lattice sites generated by plastic deformation in uniaxial shock compression; estimates of vacancy concentrations in shock-deformed silver are given. The results and interpretation are consistent with earlier shock experiments. Postshock examination of foils gives evidence for plastic deformation by slip and an estimate of final vacancy concentration.

II. EXPERIMENTAL PLAN AND PROCEDURE

In terms of a basic study of resistivity of metal under pressure, one wishes to choose a metal which typifies metallic behavior, and in as many ways as possible behaves according to simple theories. Silver was chosen since it is available in high purity, is resistant to oxidation, has no known pressure-induced phase transitions, behaves at least qualitatively according to predictions of a simple model for the pressure effect on resistivity, has a Debye temperature well below room temperature, simplifying many calculations, and has a shock impedance close to that of a readily available anvil material (Al_2O_3).

To obtain sizeable voltage drops it is necessary to use thin metal foils and high electric currents. Furthermore, for experiments to be characterized by one-dimensional compression, the specimen should be about 100 times wider than it is thick. Typical sample dimensions are shown in Fig. 1. Sample resistance at room temperature was about 5 mΩ; current was about 150 A.

High pressures for the experiments were generated by high-velocity impact. To avoid inductive coupling effects it was necessary to use nonconducting impactors. Figure 2 represents schematically the experimental configuration. Details of the projectile launching facility have been published previously.[8]

A. Specimen preparation and characterization

Specimen preparation was a multistep process involving mechanical polishing, cutting to desired shape, thickness measurement, microscope examination, annealing, resistance ratio measurements, and target assembly.

Cold-rolled silver foils were obtained from the Materials Research Corporation (MRC) and the Wilkinson Company (W3N). Mean grain size was about 75 μm in MRC foils and about 35 μm in W3N foils. There was some preferred orientation of grains due to the cold rolling. Possible influences these and other experimental details might have on results are discussed in Appendix C.

To give a uniform surface finish the foils were mechanically polished with alumina abrasive on a wheel. Foils were held flat and rigid during polishing by bonding them to quartz glass plates with phenyl salicylate. Next, specimens of desired shape were photoetched from the polished foils; a positive-working photoresist[9] and a ferric nitrate photoetch solution were used. Foil thicknesses were measured mechanically using gauge blocks and an electronic dial depth gauge; thickness variation on a foil was about ±4%. Microscope examination at 100× magnification showed faint scratches from polishing, some tarnish and occasional pits from the photoetch process, but over-all the foil surfaces were smooth and relatively stain free.

Cut foils were annealed at 800 ± 15 °K for 1—2 h in a 10^{-5}—10^{-6} Torr vacuum. Cooling took place at less than 100 °K/h.

To characterize purity and state of anneal of each foil used, specimen resistance was measured at 4.2 °K and room temperature using 2 A of current and measuring the potential drop with a Keithley 148 nanovoltmeter. Foil leads were clamped between copper blocks; current reversal was used to nullify thermal emf's. Results are shown in Table I. Spectrographic analyses were consistent with relative purity of W3N and MRC foil measured by resistance ratios; these analyses also indicated that foil surfaces were probably contaminated by Al_2O_3 particles acquired during polishing.

B. Target assembly

Target assembly involved bonding the silver specimen between sapphire anvil plates, potting the sandwich in a target holding ring, attaching electrical coaxial cables, and providing electrical shielding for the sample. Synthetic sapphire (single-crystal Al_2O_3) disks 3.8 cm in diameter and 0.3 cm thick were purchased from the Adolph Mellor Company, which specified the perpendiculars to the disk faces as oriented 50°—90° from the *c* axis of the single crystals. Sapphire is hexagonal structure so that one might expect that shock-wave propaga-

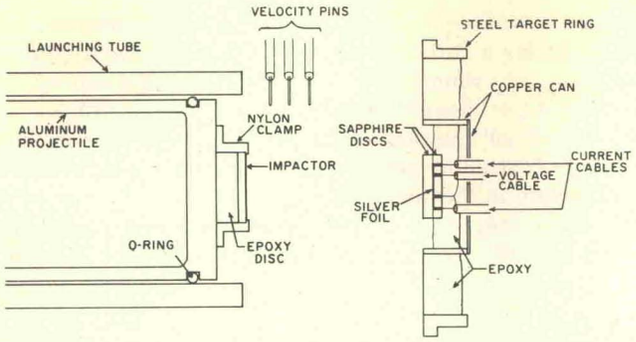

FIG. 2. Schematic diagram of impact configuration showing impactor and target assemblies.

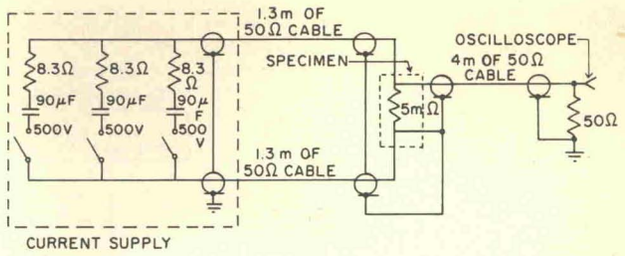

FIG. 3. Electronic measuring system.

tion would be anisotropic and mixed mode. But it has been determined experimentally that shock waves in sapphire propagate isotropically and in a pure longitudinal mode with an experimental uncertainty of $\pm 1\%$.[10] This is consistent with the experimental result that the elastic constants c_{11} and c_{33} happen to be of equal magnitude; its elastic response is symmetrical as a result.

The sapphire disk faces were parallel to within 2—10 μm. Faces were flat to within about 3 μm as observed with an optical flat and monochromatic light. As a check, the density of each sapphire disk was determined from weight measurements in air and water; the average value was 3.985 ± 0.005 g/cm^3.

Assembly involved wetting all pieces (sapphire and foil) with vacuum-outgassed epoxy (Shell Epon Resin 815). Foil leads were bent over the edges of a glass microscope slide and then pulled through the holes in the sapphire backing piece. The slide was then removed, and the front sapphire disk placed over the foil. This assembly was placed on a flat plate and screw pressure applied to a small Mylar-faced aluminum block placed on the sapphire backing piece. Lead holes were cleaned of epoxy using toothpicks soaked in acetone. After 2 h or more the holes were filled with dental amalgam which, compared to epoxy, provided a better shock-impedance match for silver and sapphire. The sandwich was visually inspected after curing to verify that the foil lay flat and to determine if there were air bubbles near the foil. The sandwich was then potted inside a copper ring which in turn had been potted into a target holding ring (Fig. 2). Next, a layer of aluminum was vacuum deposited on the target; this was done to provide a reflecting surface for optical alignment of the target on the end of the launching tube and to complete the electrical shielding with the copper ring and lid. Cables (RG-223/U) were attached and potted in place. Lengths of unshielded conductors from the plane of the foil to the coaxial cables were about 0.6 cm.

C. Impactors

Impactors for the first three shots were made of 6061-T6 aluminum. Extraneous signals were observed due to inductive coupling between sample and the metal projectile face. The remaining shots were done with a fused quartz or a sapphire impactor clamped to an aluminum projectile (Fig. 2). This eliminated inductive coupling. Impact misalignment was measured only in the first two shots. Tilt values recorded were 0.25 and 0.28 m. In the case of nonconducting impactors the projectile alignment was checked with an autocollimating telescope, the impactor face was perpendicular to the launching tube axis within 0.1—0.3 mrad. The sapphire target was also optically aligned to the tube axis. Actual tilt on impact was not recorded, since the small-diameter nonconducting impactors precluded such recording.

D. Recording system

The pulsed current source was a modified Pulsar model No. 301 power supply with three channels, each consisting essentially of a 90-μ capacitor, charged to 500 V, in series with 8.3 Ω (Fig. 3). The three channels were triggered simultaneously 15—30 μsec before impact.

Some recorded oscilloscope traces are shown in Fig. 4. One oscilloscope recorded the initial voltage step as well as voltage change across the foil upon shock compression. Two other oscilloscopes recorded only the voltage change due to shock compression. This was achieved by suppressing the initial voltage step using a differential comparator amplifier. The oscilloscopes used were 580 and 7000 series Tektronix, Inc. models; the system rise time was 4—5 nsec. Oscilloscope traces were recorded on Polaroid film. Horizontal and vertical calibrations on each shot were used to convert oscilloscope traces to voltage-time profiles

III. THEORY AND ANALYSIS

Flow of the analysis is shown in Fig. 5 and described below. From the experiment one obtains the impactor

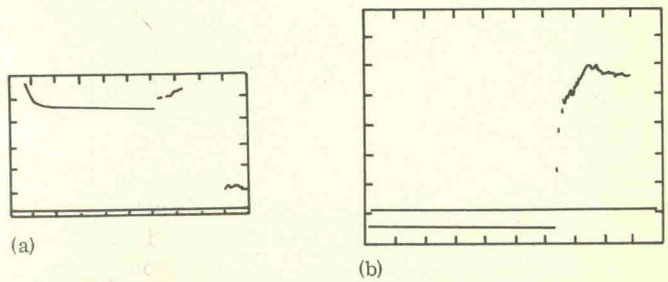

FIG. 4. Oscilloscope records. (a) Over-all record from shot 73-027 showing E_o and ΔE; 0.2 V/div, 3.5 μ sec/div. (b) Differential offset record from shot 73-050 showing ΔE vs time; 0.02 V/div, 0.2 μ sec/div.

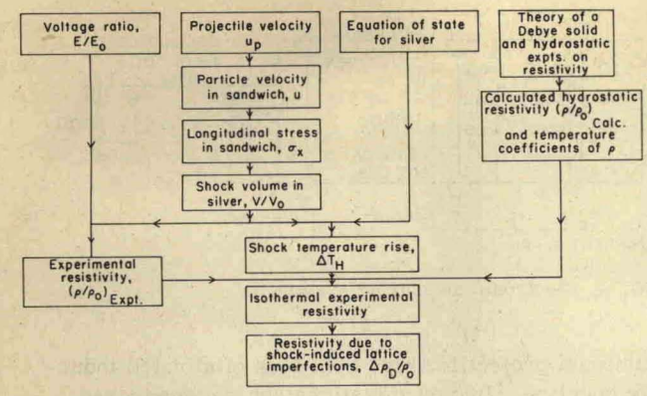

FIG. 5. Analysis flow chart.

velocity and a voltage-time profile of the shock response of the silver resistance. Known Hugoniot curves of silver and sapphire, and impactor velocity, are used to compute the pressure-volume state in silver.[11] (Computation is based on the Rankine-Hugoniot jump conditions for steady shocks.) Shock resistivity of silver is then computed. Using a P-V-T equation of state for silver fitted to experimental data, shock temperature is also calculated. Theory of a Debye solid is coupled with hydrostatic experiments on silver resistivity vs pressure to give an expression for the dependence of the temperature coefficient of resistivity on volume and to extrapolate the dependence of silver resistivity on hydrostatic pressure to 120 kbar. Then shock resistivity is corrected to isothermal conditions and compared to hydrostatic resistivity. Any deviation between shock and hydrostatic results is of interest.

A. Resistivity theory and analysis

In the Bloch-Gruneisen theory of electrical resistivity of metals[12]

$$\rho \propto T/\theta_R^2$$

for $T \gg \theta_R$ for the relation between resistivity ρ, absolute temperature T, and characteristic temperature θ_R. For an approximate treatment let us use

$$\rho = A(V)T/\theta^2(V) = \alpha(V)T, \tag{1}$$

where A is a catch-all parameter for the volume dependence of the electron band structure, Fermi geometry, Fermi energy, and details of the electron-phonon interaction, and α is the temperature coefficient of resistivity.

If we equate θ_R to θ_D, Debye temperature, then $d\ln\theta_D/d\ln V$ can be related to thermodynamic quantities, as was first noted by Gruneisen. The result is

$$\frac{d\ln\theta_D}{d\ln V} = \frac{V\alpha'}{C_V K_T} = \gamma(V), \tag{2}$$

where $\gamma(V)$ is the Gruneisen parameter, α' the volume coefficient of thermal expansion, K_T the isothermal compressibility, and C_V the constant volume specific heat.[13]

Let us consider the assumption $d\ln\theta_R/d\ln V = d\ln\theta_D/d\ln V$. Ziman[14] notes that Bloch resistivity theory is derived assuming scattering by longitudinal phonons only. So for a solid fitting the Bloch model we would expect $\theta_R = \theta_L$ which might be quite different from θ_D. Actually θ_R is close to θ_D for silver ($\theta_R = 219 \pm 20\,^\circ$K, $\theta_D = 228 \pm 3\,^\circ$K)[15] so that shear waves may participate in electron scattering processes to nearly the same extent that they do in thermal processes. Therefore, the assumption $d\ln\theta_R/d\ln V = d\ln\theta_D/d\ln V$ has some plausibility in the case of silver. Then the isothermal derivative of Eq. (1) becomes

$$\left(\frac{\partial\ln\rho}{\partial\ln V}\right)_T = 2\gamma(V) + \frac{d\ln A}{d\ln V}. \tag{3}$$

In this work we shall assume $d\ln A/d\ln V$ is constant over the range of compression studied

$$B \equiv \left.\frac{d\ln A}{d\ln V}\right|_{V=V_0} = \left(\frac{\partial\ln\rho}{\partial\ln V}\right)_{T,V=V_0} - 2\gamma(V_0).$$

Since the major dependence of ρ on volume for silver is contained in $\theta(V)$, this approximation should be adequate. Integration of Eq. (3) yields

$$\frac{\rho(V,T)}{\rho(V_0,T)} = \frac{\alpha(V)}{\alpha(V_0)} = \left(\frac{V}{V_0}\right)^B \exp\left(2\int_{V_0}^{V}\frac{\gamma(V')}{V'}dV'\right) = \left(\frac{V}{V_0}\right)^B\left(\frac{\theta}{\theta_0}\right)^{-2}. \tag{4}$$

Dugdale[16] used Bridgman's pressure derivatives for the resistance and found $B = -0.9$ for silver. Goree and Scott[17] also measured isothermal pressure derivatives of the resistivity of silver. They subtracted the pressure derivative of impurity resistivity to get the perfect lattice pressure derivative

$$\left(\frac{\partial\ln\rho_L}{\partial P}\right)_{T,P=1\text{atm}} = -4.2\times10^{-6}/\text{bar}.$$

Using Goree and Scott's derivative and $\gamma(V_0) = 2.43$, we found $B = -0.64$; this value of B was used for generating ρ on a hydrostat. [In finding $\gamma(V_0)$ ambient values of $K_T = 0.995\times10^{-6}$/bar, $\alpha' = 57.1\times10^{-6}/^\circ$K, and $C_V = 2.25$ bar cm^3/g were used.] Note that $(V/V_0)^B$, where $B<0$ tends to increase the resistivity on compression, while $(\theta/\theta_0)^{-2}$ decreases the resistivity on compression.

Experimentally metals do not exactly have resistivity proportional to absolute temperature; rather, the constant pressure resistivity is given by $\rho = \alpha T + \beta$ at high temperatures. So, to adjust theory to reality, assume $\rho = \alpha(V)T + \beta(V)$, where $\alpha(V) = A(V)/\theta^2(V)$ as before and $\beta(V)$ is an empirical parameter. From data of Kos[18] for silver $\alpha(V_0) = 0.005988$ $\mu\Omega$ cm/°K and $\beta(V_0) = -0.16$ $\mu\Omega$ cm for the range 150–300 °K.

For estimating the volume dependence of β, we use the Gruneisen-Borelius relation[19] for resistance R:

$$R_T/R_\theta = hT/\theta - (h-1), \quad h = 1.17.$$

This is an empirical relation for isotropic metals accurate in the range $0.2 < T/\theta < 1.2$. (For silver it is accurate at least to $T/\theta = 1.5$.) Ignoring thermal expansion we have $\rho_T/\rho_\theta = R_T/R_\theta$, and $\rho_T = h(T/\theta)\rho_\theta - (h-1)\rho_\theta$ in the form $\rho = \alpha T + \beta$. For silver $\rho_\theta = 1.18$

$\mu\Omega$ cm implies $\beta = -0.17\rho_\theta = -0.20$ which is close to the -0.16 value from Kos's work. Actually silver resistivity is better described using $h = 1.14$.

Now $\beta(V)$ can be found from

$$\beta = (1-h)\rho_\theta = (1-h)(\alpha\theta + \beta)$$

which gives

$$\beta(V) = [(1-h)/h]\,\alpha(V)\theta(V).$$

Finally, resistivity on the hydrostat is given by

$$\frac{\rho}{\rho_0} = \frac{\rho(V,T)}{\rho(V_0,T)} = \frac{\alpha(V)}{\alpha(V_0)}\left(1+\frac{1-h}{h}\,\frac{\theta(V)}{T}\right)\left(1+\frac{1-h}{h}\,\frac{\theta(V_0)}{T}\right)^{-1}. \quad (5)$$

Equation (5) implies that at 120 kbar for silver the empirical correction to ρ/ρ_0 as given by Eq. (1) is -2.3%.

Resistivity change due to shock temperature rise was determined from

$$\frac{\Delta\rho_T}{\rho_0} \equiv \frac{\rho(V,T)-\rho(V,T_0)}{\rho(V_0,T_0)} = \frac{\alpha(V)}{\alpha(V_0)}\left(\frac{T}{T_0}-1\right)\left(1+\frac{\beta(V_0)}{\alpha(V_0)T_0}\right)^{-1}. \quad (6)$$

(T_0 is 298 °K and V and T are volume and temperature in the shocked state.)

The isothermal shock resistivity one wishes to compare to hydrostatic resistivity [Eq. (5)] is

$$\frac{\rho(V,T_0)}{\rho(V_0,T_0)} = \frac{\rho(V,T)-\Delta\rho_T}{\rho(V_0,T_0)}. \quad (7)$$

The experiment provided $\rho(V,T)/\rho(V_0,T_0')$ data where T_0' is ambient temperature; this varied from 295.6 to 298.4 °K° The relation needed to normalize the data is

$$\frac{\rho(V,T)}{\rho(V_0,T_0)} = \frac{\rho(V,T)}{\rho(V_0,T_0')}\,\frac{\rho(V_0,T_0')}{\rho(V_0,T_0)},$$

where

$$\frac{\rho(V_0,T_0')}{\rho(V_0,T_0)} = 1 + a(T_0'-T_0), \quad a = 0.00408/°\text{K}.$$

B. Equation of state

A P-V-T equation of state for silver is needed to calculate shock temperatures and temperature coefficients $\alpha(V)$ in the compressed state; both are necessary to correct resistivity-shock pressure data to isothermal conditions. Temperature coefficients are used also in the model calculation of the resistivity of silver under hydrostatic pressure [Eq. (5)].

The equation of state chosen was an analytic fit by Zharkov and Kalinen[20] to static and dynamic P-V data. This equation of state yields a quadratic equation for temperature in the shocked state. The integration in Eq. (4) was performed using a Dugdale-MacDonald formula for the Gruneisen parameter adjusted to agree with the thermodynamic value at 1 atm; results for $\theta(V)$ were fitted to a polynomial

$$\theta/\theta_0 = 4.0465X^2 - 10.5232X + 7.4770,$$

where $X = V/V_0$. This determines numerical results for the resistivity of silver in Eqs. (4)—(6).

The above equation of state determines temperatures reached by a single shock transition from the ambient state, treating the material as a fluid. The actual temperature rise in the experiments will deviate from the simple calculation for the following reasons: (i) The final state in the experiment is not reached by a single shock but by a series of shocks because of the sandwich configuration. (ii) Heat flow from the adjacent epoxy provides additional thermal energy to the foil. (iii) Since the material has strength, there will be heat generated by the irreversible work of plastic deformation. (iv) Porosity, if present, will cause an additional temperature rise due to the extra work of compression done by the shock. These temperature deviations, if significant, will affect results for shock isothermal resistivity and defect resistivity. Reason (i) is treated below and reasons (ii)—(iv) are considered in Appendix B.

C. Reverberation temperature calculation

The sandwich configuration (anvil-foil-anvil) causes the final (P,V,T) state in the foil to be reached by a series of shock reverberations. The amount of deviation from the state reached by a single shock depends on the mechanical shock-impedance mismatch between foil and anvil. (There may also be some small reverberation effects due to the thin epoxy bonding layer.) Continuity conditions for shocks at interfaces between different materials require continuity of longitudinal stress and particle velocity normal to the interface.[11] So pressure and particle velocity in the silver are determined by the shock state in sapphire. However, the final temperature in silver has significant dependence on the shock reverberation path as opposed to a single shock path to the final state. See Appendix A for details of the calculation. For silver in sapphire, reverberation causes a smaller temperature rise than a single shock; this smaller rise by reverberation will affect the correction of shock data to isothermal resistivity by making isothermal resistivity, and hence defect resistivity, higher than if one used single-shock temperatures.

Calculations of the silver-sapphire interaction show that three wave transits are necessary to bring the silver to within 0.1% of the final shock pressure for a 100-kbar shock. In two transits it is within 0.3% and in one transit within 9%. At 100 kbar the temperature change due to reverberation shocks is 4% lower than that due to a single shock. For comparison, temperature change at 100 kbar on the isentrope centered at the initial state is about 20% lower than the single-shock temperature change.

Using the resistivity theory results, resistivity changes due to temperature rise are also calculated. Computations show that at 100 kbar the thermal resistivity change is 4% less than for a single shock. The graph of shock isothermal resistivity vs pressure is not strongly affected by the correction, but the amount of resistivity change attributed to defects generated by the

TABLE I. Results of impact experiments.

Shot No.	Foil type	Foil thickness (μm)	Foil resistance ratio $R_{4.2\,°K}/R_{296\,°K}\times10^3$	Impactor speed and type [a] (mm/μsec)	Pressure (kbar)	Voltage ratio (E/E_0 at 0.5 μsec)	Initial rise time (nsec)
72-065[b]	MRC-A[c]	16.5	3.57	0.637 Al	74.5	1.051	45
72-068[b]	MRC-A	15.6	4.17	0.853 Al	102.1	1.170	65
72-069	MRC-A	17.3	4.14	0.857 Al	103.5	1.073	35
73-009	MRC-A	14.7	4.31	0.390 S	87.1	1.049	37
73-010	MRC-A	14.3	4.38	0.392 S	87.5	1.058[d]	27
73-011	MRC-A	17.0	3.95	0.659 FQ	60.0	1.022	53
73-013	MRC-A	18.0	3.76	0.286 FQ	27.0	1.000	25
73-027	MRC-A	15.9	4.31	0.517 S	115.7	1.120	19
73-028	W3N-A	25.0	2.40	0.531 FQ	48.6	1.035	34
73-029	MRC-UA	16.1	6.85	0.562 FQ	51.8	1.032	36
73-034	MRC-UA	16.0	7.14	0.416 S	92.9	1.087	37
73-036	W3N-A	24.5	2.29	0.395 S	88.2	1.122	84
73-040	W3N-A	24.9	2.39	0.686 FQ	62.4	1.037	32
73-044	W3N-A	24.2	2.38	0.401 S	89.6	1.111	67
73-047	W3N-A	17.6	2.53	0.423 S	94.5	1.149 ± .013	• • •
73-050	W3N-A	24.0	2.25	0.524 S	117.3	1.185	34
73-051	MRC-A	16.9	4.46	0.525 S	117.5	• • •	35
73-056	MRC-A	16.6	4.18	0.89 FQ	83	• • •	• • •
73-059	MRC-A	17.2	4.48	0.530 S	118.6	1.139	34

[a] Al, FQ, and S stand for aluminum, fused quartz, and sapphire impactors, respectively.
[b] Anvils were of Lucalox.
[c] A ≡annealed, UA ≡unannealed.
[d] This value read after 0.14 μsec.

shock is about 20% higher on the MRC curve and 4.5% higher on the W3N curve after the multiple-shock calculation for the data points.

IV. RESULTS OF EXPERIMENTS AND DISCUSSION

Impact experiments were performed on 19 silver foils. Care was taken to prepare the foils in a uniform and well-characterized manner, and the experiment was designed to ensure a state of uniaxial shock compression in the silver. Data output of the impact experiments was in the form of voltage-time profiles which, when analyzed, provided resistivities of silver under shock compression. After correcting for resistivity change due to shock temperature rise, the data were compared to resistivity expected under hydrostatic pressure; from this comparison, shock-generated vacancy concentrations were estimated (Fig. 5).

In some cases postshot recovery and examination of foil pieces by optical and electron microscopy was possible. Effects of annealing on resistivity of one of the recovered foil pieces was studied also.

This section details the above results and discusses analysis of errors and possible spurious effects.

A. Summary of impact experiment results

Data were obtained on resistance changes in silver under shock compression in the pressure range from 27 to 119 kbar. Average initial temperature was 296.4 ± 0.7 °K. Resistance changes differed for silver of two different purities; higher-purity material had larger resistance changes. Annealing also appeared to affect resistance changes; unannealed foils showed slightly higher resistance changes for a given shock pressure than did annealed foils of the same purity.

Shock results, after subtracting resistivity changes due to shock temperature rise from the raw shock data (Sec. III A), are significantly higher than hydrostatic results. The difference is attributed to generation of a high concentration of vacant lattice sites by plastic deformation associated with uniaxial shock compression (see Table II). Both vacancy concentrations generated in all cases and variation of these concentrations with silver purity are difficult to understand. The higher defect resistivity observed in purer silver is opposite to results of quasistatic tensile deformation.[21]

Table I summarizes shot data. Experiments are presented in the order in which they were done. Foil type, state of anneal, foil thickness, and resistance ratio are given. Resistance ratio is the ratio of foil resistance at liquid-helium temperature to that at room temperature, and gives a relative measure of impurity and imperfection content of the foils. Resistance ratios are also affected by scattering of electrons at foil surfaces at 4.2 °K. To correct them approximately to bulk ratios using the Fuchs-Sondheimer theory[22] and a specular coefficient of 0.2,[23] multiply MRC-A ratios by 0.77, MRC-UA ratios by 0.84, and W3N-A ratios by 0.75. The average bulk resistance ratios are 0.0032 for MRC-A, 0.0059 for MRC-UA and 0.0018 for W3N-A (A and UA stand for annealed and unannealed, respectively). Measured impactor speed and type and pressure deduced from the impactor and anvil Hugoniot curves[11] are presented in columns 5 and 6, while column 7 gives the ratio of the voltage drop across the silver foil 0.5 μsec after shock arrival to the preshock voltage drop. The last column is the rise time (10—90%) of the voltage jump on shock arrival at the foil.

The first two experiments, 72-065 and 72-068, were performed using ceramic Al_2O_3 anvils; shot 72-069 used sapphire anvils. Although shots 72-068 and 72-069 were shocked to the same pressure and used silver foils

TABLE II. Results of data analysis.

Shot No.	Resistance ratio $\frac{R}{R_0}$	Resistivity ratio $\left(\frac{\rho}{\rho_0}\right)_{\text{expt}}$	Temperature rise ΔT_H (°C)	Thermal resistivity change $\frac{\Delta\rho_T}{\rho_0}$	Isothermal resistivity ratio $\frac{\rho(V,T_0)}{\rho(V_0,T_0)}$	Defect resistivity $\frac{\Delta\rho_D}{\rho_0}$
72-065	1.051	0.992	~51	0.16	0.83	• • •
72-068	1.170	1.086	~74	0.21	0.88	• • •
72-069	1.073	0.995	71.6	0.190	0.797	0.072
73-009	1.049	0.982	58.6	0.160	0.813	0.058
73-010	1.058	0.990	58.9	0.161	0.820	0.066
73-011	1.022	0.974	39.3	0.113	0.853	0.039
73-013	1.000	0.977	17.6	0.052	0.917	0.013
73-027	1.120	1.031	81.8	0.211	0.810	0.106
73-028	1.035	0.995	31.3	0.094	0.895	0.052
73-029	1.032	0.990	33.4	0.099	0.884	0.049
73-034	1.087	1.014	63.1	0.170	0.834	0.090
73-036	1.122	1.050	59.4	0.162	0.879	0.126
73-040	1.037	0.987	40.8	0.117	0.862	0.053
73-044	1.111	1.039	59.9	0.170	0.870	0.120
73-047	1.149 ± .013	1.071	63.7	0.178	0.894	0.152
73-050	1.185	1.09	82.5	0.220	0.872	0.170
73-059	1.139	1.045	84.0	0.219	0.821	0.122

cut from the same 3×5-cm foil, the resistance change was significantly larger using ceramic anvils; apparently the ceramic anvils cause extraneous deformation of the foil. The remaining experiments used polished single-crystal Al_2O_3 anvils.

To test whether observed shock-induced changes in voltage drop across a foil were due to resistance change or to artifacts, two experiments were carried out monitoring foils with no current flowing through them. No appreciable signal was observed without current flow, confirming the resistive source for voltage signals observed in the remaining experiments.

Table II presents the results of shot data analysis according to Fig. 5. The experimental resistance ratio (column 1) $R/R_0 = E/E_0$ is converted to resistivity (column 2) by

$$\frac{\rho}{\rho_0} = \frac{R}{R_0}\,\frac{V}{V_0}\,.$$

The shock temperature rise ΔT_H in column 3 is calculated as described in Sec. III C, and columns 4 and 5 give the resistivity change due to temperature rise and isothermal shock resistivity calculated from the results of Sec. III A. The last column gives the resistivity deviation between isothermal shock resistivity and calculated hydrostatic resistivity (Sec. IV D).

B. Error analysis

Contribution to errors in the analysis are found in (i) determination of the shocked state (P, V, T), (ii) recording and reading of foil resistance, and (iii) assumptions for the model describing the temperature coefficient of resistivity α as a function of volume.

Errors in determination of the shock P-V state originate in the empirical Hugoniot curve and in projectile speed. Hugoniot data for silver do not exist below 200 kbar. Hence, the portion of the curve used is an interpolation between the ambient state and data from 200 to 500 kbar. The Hugoniot curve used was from the Zharkov and Kalinen equation-of-state fit to shock data and to Bridgman's hydrostatic P-V data. Disagreement with the fit of Rice, McQueen, and Walsh[24] was 0.0005 and 0.002 in V/V_0 at 40 and 120 kbar, respectively. Uncertainties in the projectile speed are about ±0.002 mm/μsec. This uncertainty implies random uncertainty in the sapphire longitudinal stress state of ±1 kbar.

The sapphire Hugoniot itself is well established below 120 kbar and should be accurate to within ±0.5 kbar below 60 kbar and within ±1 kbar in the 60—120-kbar range. A fit by Ingram and Graham[25] for the sapphire Hugoniot, $P_x = 444\,\mu + 13.6\mu^2$, was used ($\mu$ in mm/μsec, P_x in kbar). (The Hugoniot data are for 0°, 60°, and 90° orientations relative to the c axis.)

So the final pressure state in silver is accurate to within ±1 kbar random errors and ±0.5 to 1 kbar systematic errors. The compressed volume state could be subject to a random error of ±0.001 in V/V_0 and a systematic error of up to ±0.003.

The ratio of shocked foil resistance to unshocked resistance is subject to errors in calibrating the voltage drop across the foil. The principal error source arises from recording and reading of oscilloscope traces that define the voltage. The reference voltage level E_0 should be accurate within 0.5%. Considering all elements of measurement, ΔE is accurate to about 5% and

$$\frac{E}{E_0} = 1 + \frac{\Delta E}{E_0} = \frac{R}{R_0}$$

is accurate within 0.8% for the range studied.

Calculation of temperatures in the shocked state is subject to systematic uncertainty. The thermodynamic calculation is generally accepted as valid for compressions less than 20%. However, there has been no accurate experimental confirmation of temperatures. Systematic uncertainties arise because the equation of state is fit to Hugoniot and hydrostatic compression curves; the fit is insensitive to thermal parameters. One can understand this by realizing that it would require a large temperature change to cause a 1% in-

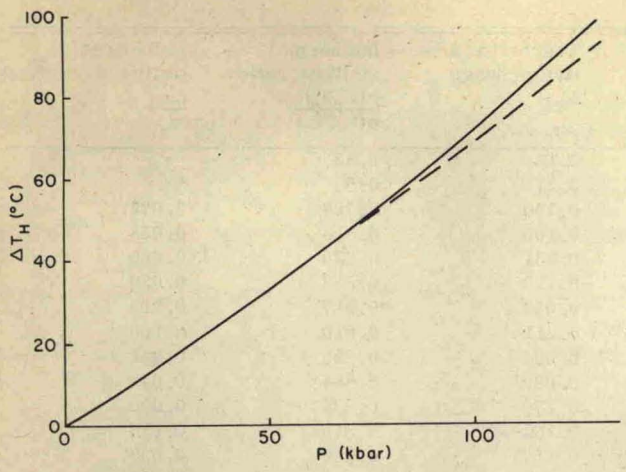

FIG. 6. Hugoniot temperature rise vs pressure. Solid line, from Zharkov and Kalinen equation of state; dashed line, from Rice, McQueen, and Walsh (Ref. 24).

crease in volume at a given pressure; for silver it would take about a 200 °K temperature change from ambient conditions. Rice, McQueen, and Walsh[24] state that calculated temperature increases should be accurate within 10%. In fact, Rice, McQueen, and Walsh's calculated temperatures agree with those from the Zharkov—Kalinen equation of state to 60 kbar and diverge to a difference of 6% at 120 kbar (Fig. 6).

The temperature coefficient of resistivity $\alpha(V)$ [Eq. (1)] and the hydrostatic pressure-resistivity curve [Eq. (5)] are calculated quantities subject to error. There are experimental data on the temperature coefficient of resistivity as a function of pressure for iron.[26] Calculated approximate coefficients,

$$\frac{\alpha}{\alpha_0} \approx \left(\frac{\theta}{\theta_0}\right)^{-2} \approx \exp\left[2\gamma_0\left(\frac{V}{V_0}-1\right)\right],$$

(here we assumed $\gamma/V = \text{const}$) are 0.4% higher at 50 kbar and 2.9% higher at 100 kbar than experimental results. (The iron data extend over a temperature range of 1000 °C.) Bridgman has also measured temperature coefficients of resistance as a function of pressure, but there are contradictions in his work. In one set of experiments he measured resistance as a function of temperature at constant pressure and in a second set he made measurements as a function of pressure at constant temperature. In the first set he measured resistance changes in noble metals over a 100 °C temperature range at constant pressure in the range 0—12 kbar.[27] The measured temperature coefficient of resistance is independent of pressure within $\frac{1}{4}\%$ ($\alpha/\alpha_0 = 1.00$). Assuming $\rho = \alpha(V)T$, this work is inconsistent with Bridgman's other work on pressure dependence of resistance at constant temperature (30 °C), where $\rho/\rho_0 = 0.956$ at 12 kbar.[28] That is to say, in the first work he found $\alpha/\alpha_0 = 1.00$ at 12 kbar, in the latter work $\alpha/\alpha_0 = 0.956$ [from Eq. (4), $\alpha/\alpha_0 = 0.96$]. This inconsistency remains if one uses Eq. (5) for relating ρ/ρ_0 and α/α_0. Based on the above discussions, accuracy of the calculated volume dependence of resistivity for silver is not well known but may be about 3% over the pressure range studied here. Until isothermal electrical resistivity and its temperature coefficient are reliably measured for silver up to 120 kbar, there remains the possibility that this part of the analysis is in serious error.

C. Voltage-time profiles

Examples of oscilloscope records of the profiles are shown in Fig. 4. The foils remain under uniaxial compression for 0.5 μsec before a rarefaction wave from the rear sapphire-epoxy interface (Fig. 2) arrives at the foil; within another 0.5 μsec rarefactions from the sapphire lateral edges also arrive. The shock-induced signal rise time is about 0.035 μsec. During the next 0.5 μsec the voltage level shows time-dependent structure. Structure depends on pressure level, silver purity, and state of anneal. That the structure is not random noise can be seen by comparing the profiles of shots 73-036 and 73-044 (Fig. 7). The two shots had the same pressure level and were the same foil type. Over-all shapes of the profiles do match roughly. The two shots were done two weeks apart, and the silver foils used were polished, photoetched, and annealed at different times. While one cannot rule out the agreement as due to reproducible artifacts of the experiment, it is tempting to ascribe the structure as due to time-dependent behavior of the silver resistivity.

Observed signal rise times range from 0.019 to 0.085 μsec, 0.035 μsec being typical. Aside from the time it takes for foil resistance to change in response to the shock transition, there are a number of experimental conditions which also affect rise time. These conditions include shock-impedance mismatch between silver and sapphire, impact misalignment, and the low-impedance epoxy layer adjacent to the foil edges. The foil reaches pressure equilibrium in about three shock transits across the foil (Sec. III. C); this takes 0.015 μsec. A typical impact misalignment of 0.3 mrad would mean a time as long as 0.013 μsec for the shock front to cross the foil. These two time effects are additive. The pressure equilibration time of about 0.05 μsec for the epoxy adjacent to the foil edges will also degrade signal rise time. The above conditions are sufficient to account for observed rise time; intrinsic response time of the resistance change is probably obscured.

D. Isothermal results

Because the shock process raises the silver tempera-

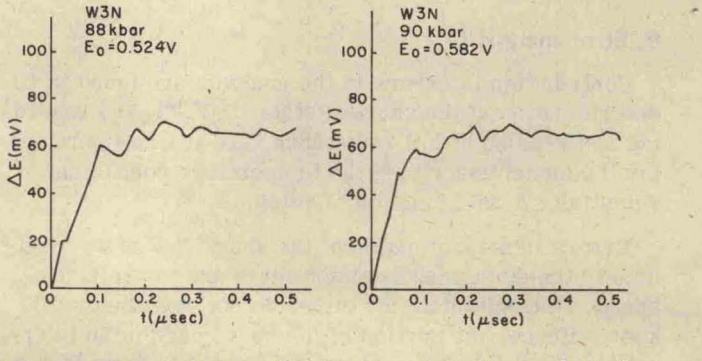

FIG. 7. Voltage-time profiles for two nearly identical shock experiments on W3N silver foils.

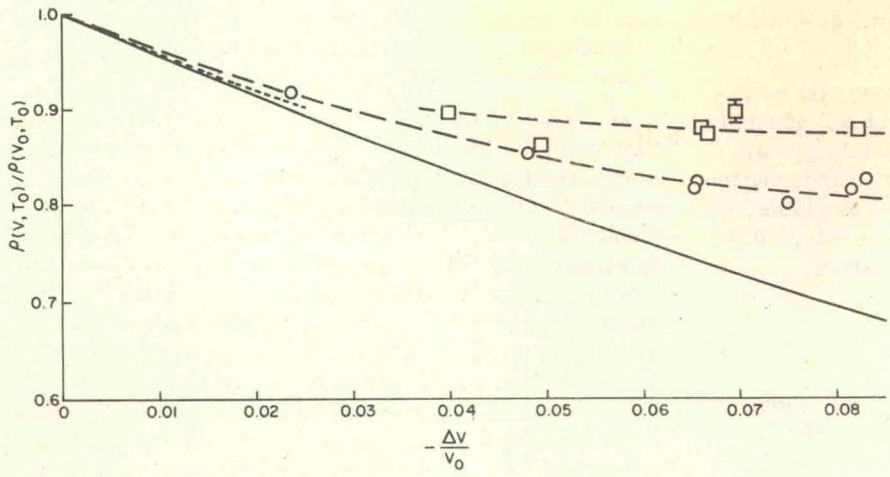

FIG. 8. Isothermal resistivity vs compression. Solid line, calculated hydrostatic resistivity fitted to initial pressure derivative of Goree and Scott (Ref. 17); dotted line, Bridgman's hydrostatic results; dashed lines, fits to experimental data of different purity; □, purer W3N silver; ○, MRC silver.

ture by an amount depending on shock strength, it is necessary to convert the shock resistance change data to isothermal resistivity before comparing them to hydrostatic experiments and theory. Conversion was done using calculations of temperature and temperature coefficient of resistance described in Sec. III.

Since the voltage-time profiles were not square pulses, some judgment was necessary in picking representative values for use in plotting data. The best-characterized point on the profile seemed to be at the end of the viewing window, $\frac{1}{2}$ μsec after shock arrival at the foil. Since on many records a more or less steady level had been reached by this time, this value was used for computing ρ/ρ_0 data points.

Isothermal resistivity of silver as a function of compression is shown in Fig. 8. All shock data lie well above the calculated hydrostat. Estimated uncertainties in temperature, temperature coefficients of resistivity, and hydrostatic resistivity extrapolation do not account for the difference. Shock results for different purity silver also differ and there may be a small effect of annealing prior to shocking for the less pure silver (Fig. 9).

Deviation of the shock isothermal resistivity from hydrostatic results is attributed mainly to resistivity of lattice defects (mainly vacancies) generated by plastic deformation associated with passage of the shock wave. This defect resistivity is given by

$$\frac{\Delta\rho_D}{\rho_0} = \frac{[\rho(V,T_0)]_{\text{Expt}} - [\rho(V,T_0)]_{\text{Calc}}}{\rho(V_0,T_0)},$$

where $[\rho(V,T_0)]_{\text{Calc}}$ comes from Eq. (5). (Also see Figs. 8 and 9.) Metals which have been shocked and relieved back to ambient conditions also show evidence of this increased lattice imperfection by changes in microstructure and hardness, and in results of annealing studies.[4–6,29–33]

If we accept the above interpretation of the deviation, the number of defects generated by the shock is quite large. Figure 9 shows the excess resistivity $\Delta\rho_D/\rho_0$ of the shock data as a function of pressure. At 100 kbar $\Delta\rho_D/\rho_0 = 0.099$ for MRC silver and 0.158 for W3N silver. In comparison, shock conductivity data of Keeler and Royce[34] for copper and iron result in $\Delta\rho_D/\rho_0 = 0.12$ and 0.16, respectively. (They corrected their data for shock temperature rise but details of the calculation were not published.)[35]

E. Defect concentrations and production

Imperfections produced by shock deformation will likely include combinations of vacancies, interstitials, dislocations, and possibly deformation twins. Experiments indicate that vacancies are formed in preference to interstitials in face-centered-cubic (fcc) metals,[4,6,31,32,36] and electron microscopy of shocked and recovered aluminum and nickel gives some evidence for prismatic dislocation loops formed by the collapse of vacancy clusters.[6,32] Of the various defects, the production of vacancies appears to be the most economical way of increasing the resistivity in fcc metals. Interstitials or dislocations require roughly three to seven times as much energy of formation as vacancies for the same resistivity change; estimates of formation energy and specific resistivity were taken from Cotterill and Doyama,[37] and Martin and Paetsch,[38] respectively, for

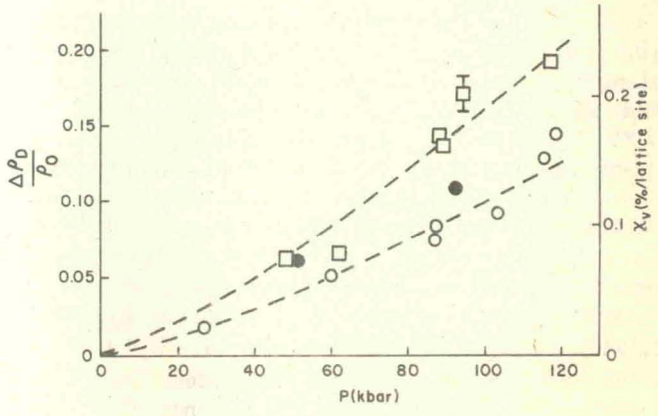

FIG. 9. Excess resistivity and vacancy concentration vs pressure. Dashed line, fit to experimental data of different purity; □, purer W3N silver; ○, annealed MRC silver; ●, unannealed MRC silver.

interstitials and from Cottrell[39] and Basinski *et al.*,[21] respectively, for dislocations.

To find approximate defect concentrations, let us assume for simplicity that excess resistivity $\Delta\rho_D$ is due to vacancies. The vacancy concentration then is $\chi_v = \Delta\rho_D/\rho_v$ where ρ_v is the resistivity per vacancy. Since vacancy resistivity as a function of pressure is not available, we will use the vacancy resistivity at 1 atm, $\rho_v = 1.3 \pm 0.7$ $\mu\Omega$ cm/at.% for silver.[40] Since $\rho_0 = 1.6$ $\mu\Omega$ cm

$$\chi_v = \frac{\Delta\rho_D}{\rho_0}\frac{\rho_0}{\rho_v} \approx 1.2\times10^{-2}\frac{\Delta\rho_D}{\rho_0}.$$

Using the 100-kbar shock data for MRC silver, computed vacancy concentration is then about 10^{-3} vacancies/atomic site (Fig. 9). Concentrations are higher in the purer W3N silver. Defect concentrations generated by severe torsion deformation or radiation damage by electrons below 20 °K are also of this magnitude.[41,42] Estimates of equilibrium vacancy concentration at the melting points of metals range as high as 10^{-2}.[43] For temperatures and pressures in shocked states of the present work, concentrations of the order of 10^{-3} correspond to strongly nonequilibrium defect concentrations. The shock experiments correspond to damage experiments at cryogenic temperatures in that defects generated do not migrate to the surface in either case. In the cryogenic case the constraint is low thermal energy of the solid; in the shock case it is the short time scale of the experiments.

For a given strain these concentrations are about two orders of magnitude higher than those found in low strain rate deformation.[44] This fact may indicate the existence of dislocation speeds near shear-wave speed since relativistic dislocations are expected to be much more efficient producers of points defects,[45] the mechanism being nonconservative motion of jogs on dislocations.[36,46]

A plot of $\ln(\Delta\rho_D/\rho_0)$ vs $\ln(-\epsilon)$ shows point-defect concentration is approximately proportional to the three-halves power of total strain ϵ; compressive strains and stresses are negative. For the expression $\chi_v = A(-\epsilon)^n$ the results for W3N silver are $A = 0.14$, $n = 1.58$ and for MRC silver are $A = 0.051$, $n = 1.46$.

F. Energy balance

One important check on the assertion that deviation from hydrostatic resistivity is due to defect resistivity is energy balance. Was enough plastic work done to generate the defect concentrations calculated in Sec. IV E? At 100 kbar an elementary calculation of work of plastic deformation[47] gives 3.9 bar cm^3/g; this was based on a Hugoniot elastic limit of 1.2 kbar calculated from a yield stress in tension of 0.5 kbar and on a work-hardening modulus of 14 kbar.[48] At 1 atm of pressure, vacancy formation energy in silver is 1.8×10^{-12} erg/vacancy.[49] As with vacancy resistivity, the dependence of monovacancy formation energy on pressure is not known. Using the 1 atm value for formation energy implies a total energy of formation of 11 bar cm^3/g for a monovacancy concentration of 10^{-3}, 2.8 times larger than the work of deformation calculated. An additional difficulty is that a majority of the work of deformation is believed to be dissipated as heat. Given these facts, an average Hugoniot elastic limit of 10—20 kbar in the first 20 μm of shock propagation in silver would be necessary to balance energy for a 100-kbar shock.

An aspect of shock response of solids which is relevant to the problem of energy balance is stress relaxation in elastic-plastic solids. For a stress relaxing solid it has been postulated that initial elastic stress in the solid at the face where the shock enters the material is equal to the total stress acting on the face, provided that the loading wave has a very fast rise time.[50] This means very high initial stresses on the dislocations in their glide planes. As the shock propagates into the material, the elastic stress relaxes with time and distance to a steady-state level characteristic of the shock response of that solid. At the same time the plastic strain is gradually accommodated by dislocation glide, multiplication, nucleation, and by twinning. If such behavior occurs in the first 20 μm of shock-wave propagation in the silver used, it is not difficult to imagine an average elastic stress over distance and time which is a sizeable fraction of a 100-kbar driving stress.

G. Effect of purity on shock-induced vacancy concentrations

Figure 9 shows the effect of purity on resistivity deviation and vacancy concentrations generated. Higher vacancy concentrations are generated in the purer silver (W3N). This effect of purity is opposite to low strain rate deformation results where, when a purity effect is noted, there is more resistivity change for lower-purity material.[51–53] Resistance ratios between room temperature and 4.2 °K indicate that W3N silver specimens have an impurity concentration about half that existing in MRC specimens. (MRC silver was specified as 5N and W3N silver as 3N pure by the supplier.)

Effect of purity has been noted in other shock experiments. Experiments in lithium fluoride by Asay *et al.*[50] showed quasistatic yield stress to increase smoothly with initial defect concentration (either impurity atoms or irradiation-induced point defects). Shock experiments by the same workers and by Gupta *et al.*[54] on the same materials showed elastic precursor decay rate and plastic strain rate to depend on concentration of divalent impurities and on heat treatment.

A model based on stress relaxation for the effect of metal purity on shock-induced defect concentrations is currently being developed by the authors.[47]

H. Effect of anneal on shock resistivity

Part of the experimental program was to determine the effect of high-temperature annealing on the resistivity change of cold-rolled silver foil in response to shock waves. Two shots were done on unannealed MRC foil. Defect concentration data for the unannealed foil are slightly higher than for annealed (Fig. 9). More data would be necessary to know if this deviation is real.

Since most point defects in silver will annihilate or diffuse to the surfaces at room temperature,[55] the main effect of high-temperature anneal is removal of disloca-

TABLE III. Results of postshock anneal.

Anneal temperature (°C)	Time duration (min)	$\frac{R_{4.2}}{R_{298}}$
Preanneal	• • •	0.0222
55—58	17	0.0232
94—97	10	0.0229
199—207	7	0.0064

tions from the cold-rolled foil; impurity clustering could also take place. Density of dislocations removed by anneal was calculated from liquid-helium-temperature resistance measurements on MRC foil before and after anneal. Using published dislocation resistivity in silver[21]

$$\Delta\rho = (1.9\times10^{-13}\,\mu\Omega\,\mathrm{cm}^3)\Lambda$$

(Λ is dislocation line density), the result was 2×10^{10} cm/cm^3. This dislocation density is within reason for cold-rolled metals; 5×10^{11}/cm^2 is quoted by Hull[56] for heavily cold-rolled metal.

Previous shock work shows a variety of effects of initial dislocation density on shock response. Work on single-crystal copper shows that 3.5% prestrain reduces the initial elastic stress jump after 5 mm of shock propagation to near zero; a ramping precursor wave then follows the jump.[57] (The prestraining increased dislocation density to 10^9 from 10^6/cm^2.) Shock hardening of annealed nickel, on the other hand, was independent of prestrain, prestrained by cold rolling to as much as 80% reduction in thickness.[58] Also, a change of an order of magnitude in initial dislocation density did not significantly affect precursor decay in lithium fluoride.[50]

From the standpoint of the jog model, one might expect greater initial forest dislocation density in unannealed foil to result in more jogs and hence more defects. This is one possible explanation of the trend of the data.

I. Discussion of resistivity time dependence

It is possible that the resistance-time structure observed for $\frac{1}{2}$ μsec in the present experiments may result from deformation processes associated with stress relaxation and possibly point-defect rearrangement and annihilation. However, enough ambiguity exists among the records to discourage detailed conjecture on the physical meaning of the resistance-time structure.

J. Work on recovered silver foil

Silver foils recovered after impact experiments were studied by observing resistance changes on annealing and by optical and scanning electron microscopy.

Pieces of silver foil up to 0.8 cm long and 0.25 cm wide were recovered in air in four shots; the shots were 73-009, 73-010, and 73-013 on MRC silver and 73-044 on W3N silver. The impact-target assembly, decelerated by nylon rags, was recovered with the silver and sapphire fragments trapped inside. Although the state of the recovered foils was affected by the relief and deceleration processes, it may give some clues to the nature of the shocked state.

A simple annealing study was made of the resistance of a foil piece recovered from shot 73-010 shocked to 87 kbar. The preshock value of the resistance ratio between liquid-helium temperature and room temperature was 0.00438. As recovered, two different foil pieces gave postshock values of 0.0222 and 0.220, five times larger than the preshock value. For shot 73-013 (27 kbar) the preshock value was 0.00376; the postshock value was 0.0178, 4.7 times as large.

The preshock resistance at 4.2 °K should be due mainly to impurities. The difference between the postshock and preshock values should be due to lattice imperfections remaining after the shock process. For shot 73-010 the resistance-ratio difference is 0.0178; for 73-013, 0.0140.

A piece from 73-010 was annealed isothermally and postanneal resistance ratios were obtained; results are given in Table III. The table shows that annealing at less than 100 °C caused almost no change in the imperfection resistance; if anything, the resistance increased slightly. (The same behavior was noted in shocked copper.[59]) Rearrangement or dispersal of imperfections could cause this. Annealing at 200 °C does remove two-thirds of the shock-induced resistivity remaining after postshot recovery. A 50 °C anneal should remove all isolated point defects created by plastic deformation.[55] Evidently any point defects generated by shock compression were able to annihilate, migrate to the surface, or cluster after relief to 1 atm in the impact experiment. The clusters, on the other hand, may be stable to higher temperatures.[60] In addition, the study of deformed silver by Bailey and Hirsch[61] indicated that dislocation density does not change until recrystallization after several hours at 208 °C. Hence, the resistivity change in the 200 °C anneal is probably due to annihilation of vacancy clusters. Using estimates by Martin and Paetsch for resistivity of clusters,[38] the vacancy concentration corresponding to the resistivity change due to the 200 °C anneal is $(0.2-0.8)\times10^{-3}$. This compares to an estimated vacancy concentration behind the shock wave of 10^{-3} for that shot.

Examination of recovered foils under an optical microscope at magnifications of 30—100 showed sets of lines locally parallel which were not present in unshocked foil. These same lines were also observed by scanning electron microscopy (Fig. 10); similar lines have been observed in shocked nickel by Dieter.[62] Dieter identifies the lines as slip bands (clusters of closely spaced slip lines). In the present work, as in the nickel work the slip bands are fragmented due to cross slip. In neither case is there evidence of deformation twins.

Average slip-band spacing in the nickel work was 2.7 ± 0.3 μm for all shock strengths (100—520 kbar). For the present work 1.4 ± 0.5 μm was a typical mean value for the observed spacing of primary slip bands. Some evidence of slip on secondary planes was observed with a spacing of about 8 μm [Fig. 10(b)]. Nickel shocked to 100 kbar showed no secondary slip, but at 460 kbar secondary slip was seen.

Dieter notes that the slip-band spacing in recovered

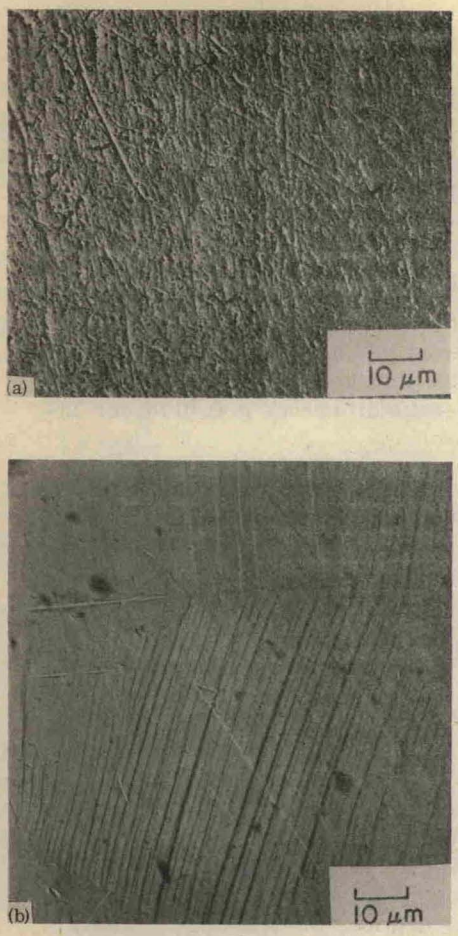

FIG. 10. Scanning electron micrographs of shocked and unshocked silver foil. (a) Unshocked MRC foil. (b) Recovered foil from shot 73-009. Note evidence of cross slip, secondary slip, and grain boundaries.

nickel may be representative only of the residual strain following shock compression and relief. The slip-band spacing observed corresponds roughly to that expected from slow deformation to the residual strain value. Similarly, observed slip-band spacing in silver is possibly typical of the final relieved state and not of the compressed state.

V. CONCLUSIONS

Accurate and reproducible measurements of resistance changes in silver foils due to shock-wave compression were accomplished. These results were made possible by careful preparation of well-characterized specimens and by careful design of the impact experiment. Experimental accuracy was sufficient to resolve an effect of silver purity on the electrical resistance or resistivity as a function of shock pressure. A smaller effect of annealing prior to shock loading also appears to be discernible. The reproducibility of the structure of voltage-time profiles obtained during the $\frac{1}{2}$ μsec of shock compression was shown in one case and consistent trends in profile shape were demonstrated in a number of other cases. The structure of the voltage-time profiles appears to depend on purity and state of anneal of the foil and on pressure.

Vacancy concentrations as high as 2×10^{-3} per lattice site were estimated from the deviation between isothermal shock resistivity data and hydrostatic results. Annealing and microscopy studies on silver foils recovered after the shock experiments tended to confirm these concentrations as well as giving evidence for dislocation slip processes. The high vacancy concentrations may be evidence for dislocation speeds near shear-wave speed. Vacancy concentrations generated were found to vary as the three-halves power of the total strain.

Calculations involved in analyzing data have themselves provided some interesting results. An approximate semiempirical calculation of resistivity vs hydrostatic pressure has been established and used to extrapolate existing experimental data beyond 30 kbar. Such calculations should prove useful in other high-pressure work.

ACKNOWLEDGMENTS

The authors are indebted to G.E. Duvall and D. Lazarus for helpful discussions. The help of P. Bellamy in operating the high-velocity impact facility and J. Guptill for technical support work is gratefully acknowledged. The work of J.J. Dick was supported by a National Defense Education Act Fellowship and the U.S. Air Force Office of Scientific Research under Contract No. 71-2037.

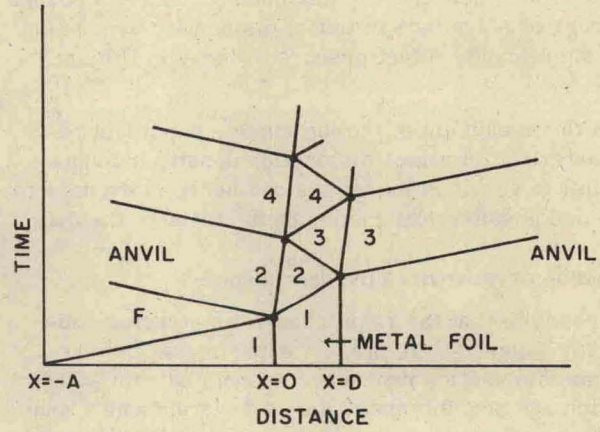

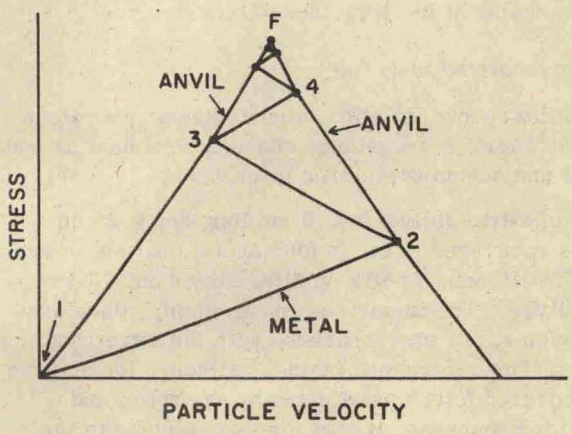

FIG. 11. Reverberation states in (t,x) and (P_x,u) planes.

APPENDIX A: SHOCK REVERBERATION ANALYSIS

The reverberation shock (P_x, u) states are found by the method of characteristics in the (P_x, u) plane. Quadratic fits, $P_x = A_i u + B_i u^2$, to the principal pressure-particle velocity curves are used in the numerical solution. (The principal Hugoniot curve through $P_x = 0$, $u = 0$ was used to generate all characteristics.) For silver, $A_1 = 3.3384$ and $B_1 = 17.448$, and for sapphire, $A_2 = 4.44$ and $B_2 = 1.36$ (P_x is in Mbar and u in cm/μsec). States in the (P_x, u) and (t, x) planes are sketched in Fig. 11.

Solution of the simultaneous equations representing the curve intersections in the (P_x, u) plane for even numbered states is different from the solution for the odd numbered states. For the nth even numbered state the quadratic equation to be solved, $au^2 + bu + c = 0$, has coefficients

$$a = B_1 - B_2,$$

$$b = A_1 + A_2 - 2B_1(u_{n-1} - u_R) + 2B_2 u_p,$$

$$c = -A_1(u_{n-1} - u_R) + B_1(u_{n-1} - u_R)^2 - A_2 u_p - B_2 u_p^2,$$

and the positive branch of the quadratic solution is used. Here u_p is twice the particle speed of the final state and u_R is the solution of $B_1 u_R^2 + A_1 u_R - P_{n-1} = 0$. For the odd numbered states,

$$a = B_1 - B_2,$$

$$b = -A_1 - A_2 - 2B_1(u_{n-1} + u_R),$$

$$c = A_1(u_{n-1} + u_R) + B_1(u_{n-1} + u_R)^2,$$

and the negative branch is used.

To find volume and temperature of a reverberation state, consider a shock from an arbitrary known initial state $(P_{n-1}, V_{n-1}, T_{n-1})$ to a final state (P_n, V_n, T_n). The Rankine-Hugoniot relation is

$$E_n = E_{n-1} + \tfrac{1}{2} V_0 (P_n + P_{n-1})(X_{n-1} - X_n),$$

where $X = V/V_0$ and E is internal energy. Also

$$E_n = E_p(X_n) + \frac{3R}{M} T_n \left(1 + \frac{1}{20} \frac{\theta_n^2}{T_n^2}\right)$$

from the equation of state (Sec. III. B), where E_p is the internal potential energy, R is the gas constant, and M is molecular weight. Hence, E_n can be eliminated between the equations and the equation for T_n becomes

$$T_n^2 - (M/3R)[E_{n-1} + \tfrac{1}{2} V_0 (P_n + P_{n-1})(X_{n-1} - X_n) - E_p(X_n)]T_n + \tfrac{1}{20}\theta_n^2 = 0.$$

Now all (P_n, V_n, T_n) reverberation states can be calculated if u_p and T_0 are given.

APPENDIX B: ADDITIONAL THERMAL EFFECTS

A. Heat flow calculation and discussion

There may be significant heat flow into the silver foil from the epoxy bonding layer during the impact experiment. Such heat flow could affect silver resistance data. Epoxy, being very compressible, gets much hotter than silver when shocked. The single-shock temperature rise at 120 kbar in epoxy is about 800 °C[63]; silver temperature rises about 90 °C and sapphire temperature about 10 °C. In these experiments, where the shocked state is reached by wave reverberations, the epoxy temprature rise is approximately 370 °C at 120 kbar.

The one-dimensional heat flow equation was solved for three slabs, epoxy-silver-epoxy. Details of the solution and computational method are given in Ref. 64. The solution does indicate significant heat flow into the silver from the epoxy in 0.5 μsec. The sandwich reaches thermal equilibrium in about 10^{-4} sec.

Accurate estimates of the temperature rise are not possible because of incomplete knowledge of epoxy thickness and of variation of the thermal conductivity of epoxy with increasing pressure and temperature. Values for these two epoxy parameters are decisive in determining the temperature rise due to heat flow in silver. Thermal conductivity of epoxy increases monotonically with pressure to 25 kbar.[65] Similarly, thermal conductivities of most dielectrics increase with temperature, but melting or decomposition might change this behavior.

Micrometer measurements of sandwich thickness indicated a total epoxy thickness of -0.5 ± 2.5 μm, the uncertainty being indicative of micrometer accuracy. This indicates a typical epoxy layer of less than 1.2 μm average thickness; perhaps about 0.6 μm is typical. One would not expect a thinner layer since the silver foil thickness measurements indicated a thickness nonuniformity of about ± 0.6 μm.

Estimated results for the temperature rise and resistivity change in silver due to heat flow $\frac{1}{2}$ μsec after shock arrival are given in Ref. 64. These estimated resistivity changes can account for some of the resistivity deviation between shock and hydrostatic results: as much as 22% in MRC silver and 9% in W3N silver. Correcting point-defect resistivity accordingly would reduce calculated magnitudes for total vacancy concentrations but would *increase* the computed concentration difference between MRC and W3N silver.

An experimental indication of heat flow effect may be present in shot 73-047 at 94 kbar. The W3N foil was thinned down to 17.6 μm from the 24.4-μm thickness of the other W3N foils; the isothermal resistivity data point without heat flow correction is indeed slightly high (Fig. 8). Heat flow correction according to Ref. 64 would bring the data point in line with the other W3N points. However, stress relaxation effects could also account for the position of that data point (Sec. IV G).

It should be noted that, in addition to other uncertainties in the calculation, the differential equation used may not completely describe the physical situation. The differential equation is a diffusion equation and neglects thermal waves which may be generated by the steep temperature gradients.[66]

B. Temperature rise due to plastic deformation and porosity

Plastic deformation is an irreversible process; the associated entropy rise increases thermal energy.[67]

Calculation shows that temperature rise in silver due to work of plastic deformation is of marginal significance for the present work; at 110 kbar the temperature rise is 2.0 °K for a maximum resolved shear stress of 0.25 kbar.[47] Since actual magnitude of resolved shear stress in silver foils in the present experiments is uncertain, the correction for this temperature rise was not applied to the data.

As little porosity as 0.1% voids would significantly affect temperature rise due to shock compression. However, transmission electron microscopy of cold-rolled metal foils shows no evidence of voids.[61]

APPENDIX C: DETAILS OF SPECIMEN CONDITION

Aside from the specimen characterization in terms of purity and anneal, there are a number of other aspects of the foil state prior to the impact experiment which should be discussed. Variations in the aspects discussed here are not believed to have significantly influenced experimental results.

A. Effects of foil thickness variation on results

Average thickness of MRC foils was 16.2 μm while for all except one of the W3N foils the average thickness was 24.4 μm. In order to check if the observed differences in experimental results between MRC and W3N-type silver were due to the differences in foil thickness, a W3N foil was thinned down to 17.6 μm. This shot, 73-047, gave resistivity results consistent with the other thicker W3N foils. We conclude that the observed difference between the two foil types is not due to different thickness.

B. Effect of specimen handling on state of anneal

Most of the experiments were done on annealed foils. The state of anneal was checked by measuring resistance at 4.2 °K. The question arises whether the state of anneal was preserved during the handling involved in target assembly. Tests were made on annealed MRC foils. To simulate assembly they were subjected to screw pressure between two glass plates wetted with acetone. One foil was also accidentally bent during this handling. Resistance at 4.2 °K was the same before and after handling within the 1% accuracy of measurement. We conclude that the state of anneal was not significantly affected by this handling.

Spot-welding silver wires to the foil tabs and soldering the wires to coaxial cables after the foil was mounted in the target did cause some transient heating but probaly did not alter significantly the state of anneal of the specimens.

C. Condition of foil surfaces

Generation of dislocations at sources on the specimen surface has been shown to be important in quasistatic deformation of silver single crystals.[68] This raises the question whether differences in surface condition could explain the differences in shock resistivity in the two silver foil types studied here. The surface state was rough and poorly defined from metallurgical and surface physics viewpoints [Fig. 10(a)]. Both foil types were prepared in nearly identical fashion except that the MRC foil, as received, had more initial surface roughness and, therefore, was mechanically polished for a longer time. Since no significant effect of surface preparation was found in the lithium fluoride precursor decay studies,[50] surface structure differences are not believed to be the cause of observed resistivity difference between foil types in the present work.

Surfaces with less roughness and less deformation could probably have been achieved using cerium oxide as the final polishing abrasive instead of the 0.05-μm alumina employed in this work. A nonmechanical polishing technique for mirror finishes developed by Henry, Hockey, and Mitchell[69] might also have improved the surface condition.

D. Grain size and preferred orientation

The mean grain sizes in the two types of silver foil used were significantly different. For annealed W3N foil, the mean grain size was about 35 μm, while for MRC foil, annealed and unannealed, it was about twice that. In both cases the mean grain size seen on the foil surface was greater than the foil thickness; we then expect that a traverse of the foil thickness is usually confined to a single grain. For this reason, the difference in grain size is not expected to have a significant effect on defect production, dislocation glide, and dislocation generation. One can envision some effect on dislocations moving on glide planes at large angles to the shock direction; such dislocations might reach and interact with grain boundaries.

It should be noted that there is some effect of grain size on yield stress at low strain rates.[70] A factor-of-2 increase in grain size in silver causes an 8% decrease in yield stress. However, in shock experiments no effect of grain size on HEL after 19 mm of shock propagation was noted in Armco iron.[71] An effect of grain size on precursor attenuation in the first mm or less of shock propagation cannot be ruled out. Lithium fluoride work showed no effect of the number of subgrain boundaries on the precursor decay or HEL,[50] whereas in copper there was an effect.[57] Grain size is thus a possible, but not likely, source of the difference in defect resistivity between the two foil types.

This is an appropriate time to discuss preferred orientation of crystallites in cold-rolled foils. The topic has been reviewed by Barrett and Massalski.[72] For silver rolled at room temperature or below the texture is described by the (110) plane parallel to the rolling plane and the $[1\bar{1}2]$ direction parallel to the rolling direction. Other crystallite orientations are present but with less frequency.

Rolling texture changes to a new texture on low-temperature annealing but becomes random with annealing above 800 °C. After long annealing at 433 to 533 °C (anneals in present work were 1–2 h at 535 °C the orientation is the same as the original rolling texture.

Based on the above discussion, it is most likely that

the silver foils used in the present work had a (110) [$1\bar{1}2$] texture.

Barrett and Massalski observed that in fcc metals the predominant dislocation slip plane is the closest-packed (111) plane. Many metals alter their slip plane at high or low temperature or high strain rate. In copper and tungsten, however, the same slip systems operate under shock as in quasistatic deformation.[57,73] For crystallites with (110) planes parallel to the foil surfaces, three (111) planes will be at 45° to the foil surface. The maximum resolved shear stress in uniaxial shock compression is approximately at 45° to the foil surface, so that dislocations on (111) slip planes would be subjected to this maximum shear stress $\frac{1}{2}(\sigma_x - \sigma_y)$. This leads us to observe that differences in crystallite preferred orientation in the two types of foil studied could lead to differences in defect production by the shock. No such differences in crystallite orientations are expected, however.

*Present address: Battelle Research Laboratories NW, Richland, Wash. 99352.

[1]W. Paul, *High Pressure Physics and Chemistry*, edited by R. S. Bradley (Academic, London, 1963), Vol. 1, pp. 299-354.
[2]P. W. Bridgman, Proc. Am. Acad. Arts Sci. **81**, 167 (1952).
[3]D. L. Styris and G. E. Duvall, High Temp.-High Press. **2**, 477 (1970).
[4]H. Kressel and N. Brown, J. Appl. Phys. **38**, 1618 (1967).
[5]S. Mahajan, Phys. Status Solidi A **2**, 187 (1970).
[6]F. E. van Wely, *Behaviour of Dense Media under High Dynamic Pressures* (Gordon and Breach, New York, 1968), pp. 337-342.
[7]M. J. Ginsberg and D. E. Grady, Bull. Am. Phys. Soc. **17**, 1100 (1972).
[8]G. R. Fowles, G. E. Duvall, J. Asay, P. Bellamy, F. Feistmann, D. Grady, T. Michaels, and R. Mitchell, Rev. Sci. Instrum. **41**, 984 (1970).
[9]Shipley Co., AZ-111.
[10]R. E. Graham and G. E. Ingram, *Behaviour of Dense Media under High Dynamic Pressures* (Gordon and Breach, New York, 1968), pp. 469-482.
[11]G. R. Fowles, *Dynamic Response of Materials to Intense Impulsive Loading*, edited by P. C. Chou and A. K. Hopkins (Wright-Patterson Air Force Base, Ohio, 1972), pp. 405-480.
[12]N. F. Mott and H. Jones, *The Theory of Metals and Alloys* (Oxford U. P., London, 1936).
[13]M. H. Lenssen and A. Michels, Physica **2**, 1091 (1935).
[14]J. M. Ziman, *Electrons and Phonons* (Oxford U. P., London, 1960), p. 370.
[15]K. A. Gschneidner Jr., *Solid State Physics*, edited by F. Seitz and D. Turnbull (Academic, New York, 1964), Vol. 16, pp. 276-426.
[16]J. B. Dugdale, Science **134**, 77 (1961).
[17]W. S. Goree and T. A. Scott, J. Phys. Chem. Solids **27**, 835 (1966).
[18]J. F. Kos, Can. J. Phys. **51**, 1602 (1973).
[19]A. N. Gerritsen, *Encyclopedia of Physics*, edited by S. Flugge (Springer-Verlag, Berlin, 1956), Vol. **19**, p. 170.
[20]V. N. Zharkov and V. A. Kalinèn, *Equations of State for Solids at High Pressures and Temperatures* (Consultants Bureau, New York, 1971).
[21]Z. S. Basinski, J. S. Dugdale, and A. Howie, Philos. Mag. **8**, 1989 (1963).
[22]E. H. Sondheimer, Adv. Phys. **1**, 1 (1952).
[23]V. P. Nagpal and V. P. Duggal, Thin Solid Films **9**, 313 (1972).
[24]M. H. Rice, R. G. McQueen, and J. M. Walsh, *Solid State Physics*, edited by F. Seitz and D. Turnbull (Academic, New York, 1958), Vol. 6, pp. 1-63.
[25]G. E. Ingram and R. A. Graham, Fifth Symposium of Detonation, 1970, pp. 369-386 (unpublished).
[26]E. V. Clougherty and L. Kaufman, *High Pressure Measurement*, edited by A. A. Giardini and E. C. Lloyd (Butterworths, Washington, 1963), pp. 152-163.
[27]P. W. Bridgman, *The Physics of High Pressure* (G. Bell and Sons, London, 1958).
[28]P. W. Bridgman, Proc. Am. Acad. Arts Sci. **72**, 157 (1938).
[29]O. E. Jones, *Third Internationational Conference on High Pressure-Engineering Solids under Pressure* (Institute of Mechanical Engineers, London, 1970), pp. 75-86.
[30]A. H. Jones, C. J. Maiden, and W. M. Isbell, *Mechanical Behaviour of Materials under Pressure*, edited by H. Li. D. Pugh (Elsevier, Amsterdam, 1970), pp. 680-747.
[31]A. Christou, Scr. Metall. **5**, 749 (1971).
[32]M. F. Rose and T. L. Berger, Philos. Mag. **17**, 1121 (1968).
[33]Present paper, see Sec. IV J.
[34]R. N. Keeler and E. B. Royce, *Physics of High Energy Density* (Academic, New York, 1971), p. 121.
[35]R. E. Duff, *Properties of Matter under Unusual Conditions*, edited by H. Mark and S. Fernbach (Interscience, New York, 1969). p. 93.
[36]F. R. N. Nabarro, *Theory of Crystal Dislocations* (Oxford U. P., London, 1967).
[37]R. M. J. Cotterill and M. Doyama, in *Lattice Defects and Their Interactions*, edited by R. R. Hasiguti (Gordon and Breach, New York, 1967). p. 160.
[38]J. W. Martin and R. Paetsch, J. Phys. F **3**, 907 (1973).
[39]A. H. Cottrell, *Dislocations and Plastic Flow in Crystals* (Clarendon Press, Oxford, 1953), p. 38.
[40]R. W. Balluffi, J. S. Koehler, and R. O. Simmons, in *Recovery and Recrystallization in Metals*, edited by L. Himmel (Gordon and Breach, New York, 1963), p. 18.
[41]F. Thom, Phys. Status Solidi B **49**, K111 (1972).
[42]H. Wagner, F. Dworschak, and P. Wombacher, in *First European Conference on Condensed Matter* (European Physics Society, Geneva, 1971), p. 68.
[43]Ya. A. Kraftmakher and P. G. Strelkov in *Vacancies and Interstitials in Metals*, edited by A. Seeger, D. Schumacher, W. Schilling, and J. Diehl (North-Holland, Amsterdam, 1968), pp. 59-78.
[44]A van den Beukel, in *Vacancies and Interstitials in Metals*, edited by A. Seeger, D. Schumacher, W. Schilling, and J. Diehl (North-Holland, Amsterdam, 1968), pp. 427-479.
[45]J. Weertman, in *Response of Metals to High Velocity Deformation*, edited by P. G. Shewmon and V. F. Zackay (Interscience, New York, 1961), pp. 205-247.
[46]F. Seitz, Adv. Phys. **1**, 43 (1952).
[47]J. Dick, Ph. D. thesis (Washington State University, 1974) (unpublished); WSU-SDL Report No. 74-01 (unpublished).
[48]H. I. Dawson, Physica 31, 344 (1965).
[49]J. S. Koehler, in *Vacancies and Interstitials in Metals*, edited by A. Seeger, D. Schumacher, W. Schilling, and J. Diehl (North-Holland, Amsterdam, 1968), p. 175.
[50]J. R. Asay, G. R. Fowles, G. E. Duvall, M. H. Miles, and R. F. Tinder, J. Appl. Phys. **43**, 2132 (1972).
[51]T. H. Blewitt, R. R. Coltman, and J. K. Redman, in *Report of the Conference of Defects in Crystalline Solids* (The Physical Society, London, 1955), pp. 369-382.
[52]K. Tanaka and T. Watanabe, Jpn. J. Appl. Phys. **11**, 1429 (1972).
[53]Z. S. Basinski and S. Saimoto, Can. J. Phys. **45**, 1161 (1967).
[54]Y. M. Gupta, G. R. Fowles, and G. E. Duvall, J. Appl. Phys. 46, 532 (1975).
[55]H. I. Dawson, Acta Metall. **13**, 453 (1965).
[56]D. Hull, *Introduction to Dislocations* (Pergamon, Oxford, 1965).
[57]O. E. Jones and J. D. Mote, J. Appl. Phys. **40**, 4920 (1969).
[58]M. F. Rose, T. L. Berger, and M. C. Inman, Trans. AIME **239**, 1998 (1967).
[59]D. C. Brillhart, A. G. Preban, and P. Gordon, Met. Trans.

1, 969 (1970).
[60]B. L. Eyre, J. Phys. F 3, 422 (1973).
[61]J. E. Bailey and P. B. Hirsch, Philos. Mag. 5, 485 (1960).
[62]G. E. Dieter, in *Response of Metals to High Velocity Deformation*, edited by P. G. Shewmon and V. F. Zackay (Interscience, New York, 1961), pp. 409-444.
[63]R. G. McQueen, S. P. Marsh, J. W. Taylor, J. N. Fritz, and W. J. Carter, *High Velocity Impact Phenomena*, edited by R. Kinslow (Academic, New York, 1970), p. 557.
[64]G. W. Swan and J. J. Dick, J. Appl. Phys. 45, 3851 (1974).
[65]P. Andersson and G. Backstrom, J. Appl. Phys. 44, 2601 (1973).
[66]P. M. Morse and H. Feschbach, *Methods of Theoretical Physics* (McGraw-Hill, New York, 1953), p. 865.
[67]G. E. Duvall, *Dynamic Response of Materials to Intense Impulsive Loading*, edited by P. C. Chou and A. K. Hopkins (Wright-Patterson Air Force Base, Ohio, 1972), pp. 89-122.
[68]F. J. Worzala and W. H. Robinson, Philos. Mag. 15, 939 (1967).
[69]L. F. Henry, B. J. Hockey, and J. W. Mitchell, Rev. Sci. Instrum. 41, 1549 (1970).
[70]E. O. Hall, *Yield Point Phenomena in Metals and Alloys* (Macmillan, London, 1970), pp. 37ff.
[71]O. E. Jones and J. R. Holland, Acta Metall. 16, 1037 (1968).
[72]C. S. Barrett and T. B. Massalski, *Structure of Metals* (McGraw-Hill, New York, 1966).
[73]T. E. Michaels, Ph. D. thesis (Washington State University, 1972) (unpublished).